A proof-of-principle experiment on a new diagnostic tool for determining beam sizes from angular distributions of parametric X-ray radiation

A.V. Berdnichenko [a], Yu.A. Goponov [a], R.A. Shatokhin [a], Y. Takabayashi [b], I.E. Vnukov [a],*

[a] Belgorod National Research University, 85 Pobedy str., 308015 Belgorod, Russia
[b] SAGA Light Source, 8-7 Yayoigaoka, Tosu, Saga 841-0005, Japan

ARTICLE INFO

ABSTRACT

A previously proposed technique for measuring the transverse sizes of an electron beam was verified experimentally by comparing the angular distributions of parametric X-ray radiation in a thin crystal for two distances between the crystal and the detector. The measurements were performed on a 255-MeV electron beam incident on a 20 μm-thick silicon crystal. The angular distributions of parametric X-ray radiation were measured using an imaging plate as a two-dimensional position-sensitive detector. The obtained horizontal and vertical beam sizes were in good agreement with the results of measurements by optical transition radiation. The proposed method would be useful for electron beam diagnostics for recently advanced linear accelerators where optical transition radiation cannot be used as a beam profile monitor owing to the coherent effect.

1. Introduction

For electron linear accelerators, visible light from a fluorescent screen or optical transition radiation (OTR) [1] from a metal foil is often used for beam profile monitors. In particular, OTR monitors have been employed as a reliable high-precision tool for measuring beam profiles in many accelerator facilities. However, it has been reported that the OTR intensity is not proportional to the beam intensity and fluctuates shot by shot due to the coherent effect, i.e., beam profiles cannot be obtained from the OTR measurements for linear accelerators dedicated to X-ray free-electron lasers (XFEL) [2], because the bunch length (longitudinal beam size) is ultrashort and approaches the wavelength of the observed radiation [3]. For electron (positron) beams with ultrasmall transverse sizes comparable to the wavelength of the observed radiation, e.g., at electron–positron linear colliders [4,5], a similar coherent effect would be expected to occur.

One of solutions to this problem is to employ radiation with a shorter wavelength, and some groups, including ours, have proposed the application of parametric X-ray radiation (PXR) [6,7] to beam profile monitors. When relativistic charged particles are incident on a single crystal, PXR is emitted in the Bragg direction and can be regarded as the diffraction of virtual photons associated with the incident particles ([8–13] and the literature cited therein). Since its first observation in the 1980's, PXR has been investigated theoretically and experimentally, and some groups have performed studies applying PXR as a new wavelength-variable monochromatic X-ray source [14,15]. A number of experiments on beam diagnostic methods using PXR have also recently been performed [7,16,17].

In [18,19], we proposed a new method for determining electron beam sizes from PXR angular distributions for two distances between the crystal and the position-sensitive X-ray detector. In [19], it was shown that the minimum beam sizes $\sigma_{x,y}$ measured using the proposed method are determined by the conditions $\sigma_{x,y} > \delta$ and $\sigma_{x,y}/R > 0.1\Theta_{\text{ph}}$, where δ is the pixel size of the detector and R is the distance between the crystal and the detector. The characteristic angle of the RXR angular distribution can be written as $\Theta_{\text{ph}} = \sqrt{\gamma^{-2} + (\hbar\omega_{\text{p}}/\hbar\omega)^2} \approx$ 2–5 mrad [13], where γ is the Lorentz factor, $\hbar\omega$ is the X-ray energy, and $\hbar\omega_{\text{p}}$ is the plasmon energy for the crystal. The measurable minimum beam sizes are estimated to be 50–60 μm [19]. For electron energies above 5 GeV, the PXR contribution in the Bragg direction is negligible, and the contribution of diffracted transition radiation (DTR) with a characteristic angle $\Theta_{\text{ch}} \sim \gamma^{-1}$ becomes dominant [20]. In this case, DTR can be used instead of PXR, and the measurable beam size is limited by the pixel size of the detector and comparable to 10–15 μm [19]. Following the work [18,19], we discussed the scheme for determining beam sizes for XFEL linear accelerators [21], and the scheme for determining emittances of 5–10 GeV electron beams [22].

In this work, we have demonstrated a proof-of-principle experiment on the method for determining transverse beam sizes from PXR angular distributions measured for two crystal-detector distances, as proposed in [18,19]. The measured values are compared with those obtained by a conventional method by OTR and the validity of the present method is discussed.
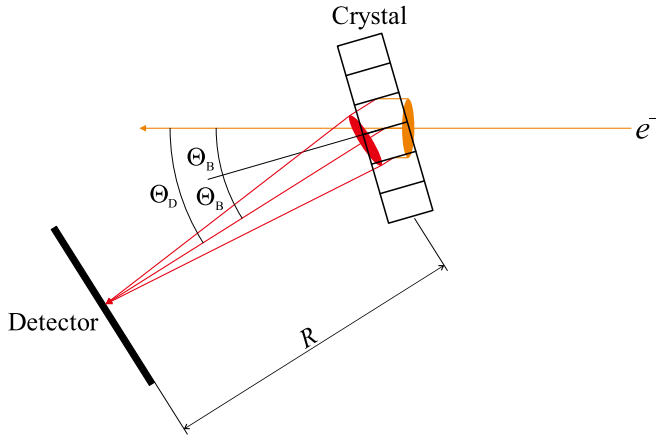
Fig. 1. Schematics of proposed method.

2. Principle of the proposed method

Here, we briefly describe the principle of the proposed method, since the details are already discussed in [18,19]. Fig. 1 illustrates the proposed method. A position-sensitive X-ray detector is placed in the Bragg direction ($2\Theta_B$ with respect to the beam direction) at a distance R from the crystal. As shown in Fig. 1, the effective size of the PXR source on the target corresponds to that of the electron beam in the case of such a symmetrical Laue arrangement. The PXR angular distribution to be observed at the detector is blurred depending on the beam size and the distance between the crystal and the detector. For $R \to \infty$, the PXR angular distribution to be observed at the detector converges to that from a point-like source.

The PXR angular distribution from a beam with a finite size can be written as:

$$Y(\theta_y, \theta_x) = \iint Y(\theta'_y, \theta'_x) G(\theta'_y \to \theta_y, \theta'_x \to \theta_x) d\theta'_y d\theta'_x, \quad (1)$$

$$G(\theta'_y \to \theta_y, \theta'_x \to \theta_x) =$$

$$\frac{1}{2\pi\sigma'_y\sigma'_x} \exp\left[\frac{-(\theta_y - \theta'_y)^2}{2(\sigma'_y)^2}\right] \exp\left[\frac{-(\theta_x - \theta'_x)^2}{2(\sigma'_x)^2}\right], \quad (2)$$

where $Y(\theta'_y, \theta'_x)$ is the angular distribution for a point-like beam, $\sigma'_{x,y} = \sigma_{x,y}/R$ are the effective divergence angles in the horizontal and vertical directions, and $\sigma_{x,y}$ are the horizontal and vertical beam sizes on the target.

The two-dimensional angular distribution $Y_R(\theta_{y_i}, \theta_{x_j})$ measured by a detector at a distance R from the crystal can be expressed as follows:

$$Y_R(\theta_{y_i}, \theta_{x_j}) = \int\int_{\Delta\Omega(y_i, x_j)} Y_R(\theta_y, \theta_x) d\theta_y d\theta_x, \quad (3)$$

where $Y_R(\theta_y, \theta_x)$ is defined by Eqs. (1) and (2), and $\Delta\Omega(y_i, x_j)$ is the solid angle spanned by the detector element located at the point (y_i, x_j) on the two-dimensional detector.

In the present method, PXR angular distributions are measured at two distances R_1 and R_2 from the crystal, where $R_1 = k \cdot R_2$. We can assume that $Y_{R_2}(\theta_{y_i}, \theta_{x_j})$ is written as a convolution of the distribution $Y_{R_1}(\theta_{y_i}, \theta_{x_j})$ with Gaussian functions having dispersions $\widetilde{\sigma}'_{x,y}$. To determine $\widetilde{\sigma}'_{x,y}$, we employ the least-squares method to minimize the following equation:

$$\sum_{i=1}^{n}\sum_{j=1}^{m}\left[Y_{R_2}(\theta_{y_i}, \theta_{x_j}) - \frac{1}{2\pi\widetilde{\sigma}'_x\widetilde{\sigma}'_y}\sum_{i'=1}^{n}\sum_{j'=1}^{m}Y_{R_1}(\theta_{y_{i'}}, \theta_{x_{j'}})\right.$$

$$\left.\exp\left(-\frac{(\theta_{y_i} - \theta_{y_{i'}})^2}{2(\widetilde{\sigma}'_y)^2}\right)\exp\left(-\frac{(\theta_{x_j} - \theta_{x_{j'}})^2}{2(\widetilde{\sigma}'_x)^2}\right)\right]^2 = \text{Min.}, \quad (4)$$
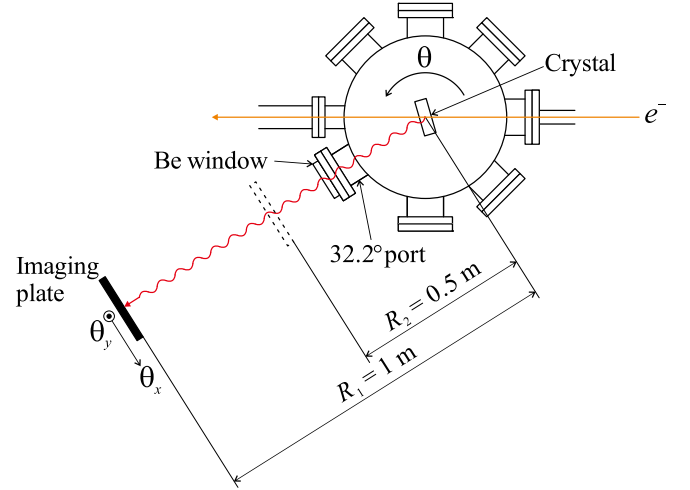
Fig. 2. Schematic of experimental setup (top view).

where $\widetilde{\sigma}'_x$ and $\widetilde{\sigma}'_y$ are fitting parameters, and m, n are numbers of the detector elements (pixels). The beam sizes σ_x and σ_y can be derived as [18]:

$$\sigma_{y,x} \approx \frac{k \cdot R_2}{\sqrt{k^2 - 1}}\widetilde{\sigma}'_{y,x}. \quad (5)$$

3. Experimental

The experiment was performed using a 255-MeV ($\gamma \sim 500$) electron beam from the linear accelerator of SAGA Light Source (SAGA-LS) in Japan. The pulse repetition rate was 1 Hz, and the average beam current was ~7 nA. The divergence of the electron beam was $\vartheta_{x,y} \approx 0.1$ mrad in terms of one standard deviation. The horizontal and vertical beam sizes on the target were measured using OTR [16] to be $\sigma_x = 0.28 \pm 0.01$ mm and $\sigma_y = 1.33 \pm 0.02$ mm, respectively, in terms of one standard deviation.

The experimental setup is illustrated in Fig. 2. A 20-μm-thick silicon crystal was mounted on a two-axis goniometer in a vacuum chamber. The <001> axis was perpendicular to the crystal surface, which was set so that the (110) plane perpendicular to the crystal surface would be directed vertically. To register PXR on the (110) plane, the crystal was rotated by an angle $\theta = \Theta_B = 16.1°$ (the normal incidence condition is defined as $\theta = 0°$). The radiation generated in the crystal passed through a 250-μm-thick beryllium window and was recorded by a two-dimensional position-sensitive detector located at an angle $\Theta_D = 32.2°$.

As a detector, we used an imaging plate with dimensions of 250×200 mm^2, a chemical composition of BaSrFBrI:Eu^{2+} and a working layer thickness of 112 μm (type IPU, manufactured by Baker Hughes) [23]. As shown in [24], such plates are very convenient for observing the PXR angular distributions because of their large area, high spatial resolution, and the linear dependence of the degree of local ionization in the plate material on the intensity of the detected radiation. During X-ray irradiation with the plate, Eu^{2+} was ionized to Eu^{3+}, and the released electrons were captured by lattice defects [23,25]. After exposure of the plate to the photon beam, the latent X-ray image was read digitally by a photo-stimulated luminescence process using an imaging plate reader (CRxVision, Baker Hughes). It takes a few minutes for this reading process. The pixel size in the imaging plate was 35×35 μm^2. In our experimental setup, the distance between the crystal and the output window of the accelerator vacuum chamber was 0.33 m. Taking into account the need to install a Kapton absorber and additional shielding of the imaging plate from the background (see below), we

chose distances between the crystal and the detector as $R_2 = 0.5$ m and $R_1 = 1$ m. For imaging plates, X-ray images stored in the detector are not observed during irradiation, and the detector sensitivity is lower than that for solid-state detectors such as X-ray CCD cameras. For automation of the measurements, such solid-state detectors would therefore be useful.

The background conditions depend on the operating mode of the accelerator, the location of the detector, and the crystal orientation angle [26]. To determine the angular distribution of the background for each of the distances, the crystal was misoriented by $\pm 3°$ from the Bragg angle. As the background distribution, we took the average of the distributions for these crystal misorientation angles. The background intensity did not exceed 20%–30% of the peak intensity of the PXR angular distribution.

The photon path length in vacuum was 0.33 m; therefore, the path lengths in air were 0.17 m and 0.67 m for $R_2 = 0.5$ m and $R_1 = 1$ m, respectively. The radiation recorded by the detector installed at a distance $R_1 = 1$ m was absorbed more strongly than the radiation recorded at a distance $R_2 = 0.5$ m. To compensate for this difference, a 675-μm-thick Kapton film was installed in front of the detector at $R_2 = 0.5$ m. The difference in transmission fraction, $T = \exp(-\mu t)$, where μ is the linear absorption coefficient [27] and t is the length of the radiation path in the substance, between a 0.5-m-thick layer of dry air and the 675-μm-thick Kapton film does not exceed 0.5%–1% for the photon energies of the three most intense orders of reflection: (220), (440), and (660).

4. Results and discussion

Fig. 3 shows the observed PXR angular distributions for $R_1 = 1$ m and $R_2 = 0.5$ m, with the background not subtracted. The Bragg direction corresponded to $\theta_x = \theta_y = 0$. The measurement time for each distribution was 600 s.

Fig. 4 shows the cross-sections of the obtained angular distributions passing through the center of the PXR reflection in the horizontal and vertical directions for distances of 0.5 and 1 m, with the background subtracted. The areas of the detector elements were taken to be 35×35 μm^2 and 70×70 μm^2 for $R_2 = 0.5$ m and $R_1 = 1$ m, respectively, to match their solid angles.

It can be seen from the figure that the distributions for different distances practically coincide, except for the region near the reflection center $\theta_{x,y} < 7$–8 mrad, where the distribution for $R_1 = 1$ m is much more prominent. Vertical distributions differ more, since the vertical beam size is significantly larger than the horizontal one.

Determination of the beam size via Eqs. (4) and (5) was carried out by varying the convolution parameters $\tilde{\sigma}'_{x,y}$ using the Monte Carlo method. The fitting region of ± 25 and ± 20 mrad relative to the reflection center for the horizontal and vertical directions was chosen so that the loss of radiation intensity at the edges of the distributions due to smoothing would not affect the reliability of the fitting results. Fig. 5 shows the horizontal and vertical sections of the measured dependence $Y_{R_2}(\theta_{y_i}, \theta_{x_j})$ (triangles) and the fitted dependence (solid curve), as well as the difference between them (circles).

As can be seen in Fig. 5, the fitted dependence coincides quite well with $Y_{R_2}(\theta_{y_i}, \theta_{x_j})$, and their difference is roughly symmetric with respect to zero, except for the region $|\theta_y| > 25$ mrad, where there is a decrease in the fitting distribution due to smoothing effects. At the same time, it should be noted that the fitting dependence is slightly higher than $Y_{R_2}(\theta_{y_i}, \theta_{x_j})$ at the center of the PXR reflection.

The resulting beam sizes were $\sigma_x = 0.32 \pm 0.02$ mm and $\sigma_y = 1.35 \pm 0.02$ mm, where we took the scatter in the beam sizes obtained in a series of repeated fittings as an estimate of the error in the fitting results. The values obtained are in satisfactory agreement with the results of measurements with optical transition radiation: $\sigma_x = 0.28 \pm 0.01$ mm and $\sigma_y = 1.33 \pm 0.02$ mm. In this type of method integrating many beam shots to obtain beam sizes, as in the case of wire scanners,
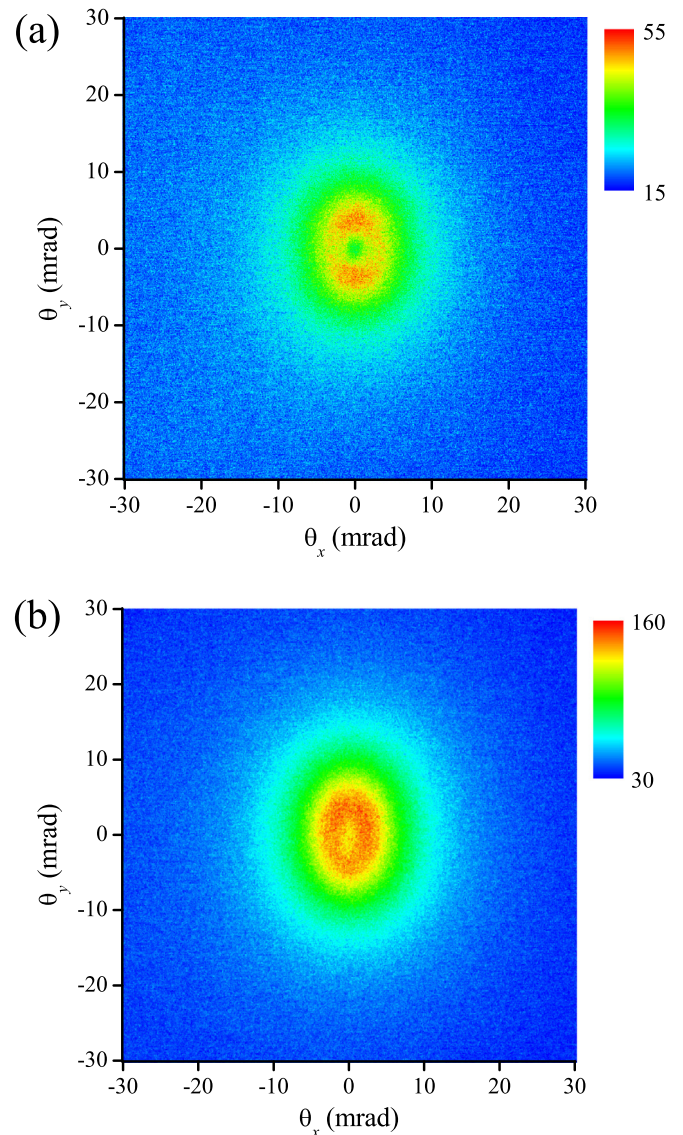
Fig. 3. PXR angular distributions observed for (a) $R_1 = 1$ m and (b) $R_2 = 0.5$ m.

the stability of the beam position affects the beam size measurements. The beam position fluctuation was approximately 1% of the beam size, and thus its effect was negligible under the present experimental conditions. However, for smaller beam sizes, this may have an effect on the measurement results.

The difference between the beam sizes obtained using different techniques, as well as the previously noted difference between $Y_{R_2}(\theta_{y_i}, \theta_{x_j})$ and the fitted dependence, may be due to experimental errors and the incomplete compensation of radiation absorption in a 0.5-m-thick layer of air in the case of the Kapton film. The ratios of the radiation transmission fractions in the 675-μm-thick Kapton film and the 0.5-m-thick air layer vary from 0.995 to 0.991 for photons with energies $\omega \approx$ 11.64 keV, 23.29 keV, and 34.93 keV for the (220), (440), and (660) reflections, respectively. That is, the angular distribution $Y_{R_2}(\theta_{y_i}, \theta_{x_j})$ obtained using the Kapton film has a lower intensity than that obtained if the experimental conditions are identical in both measurements, with the exception of the distance between the crystal and coordinate detector. To compensate for this difference, the fitting program overestimates the effective divergence and the resulting beam sizes. It should be noted here that the PXR photon energy depends on the
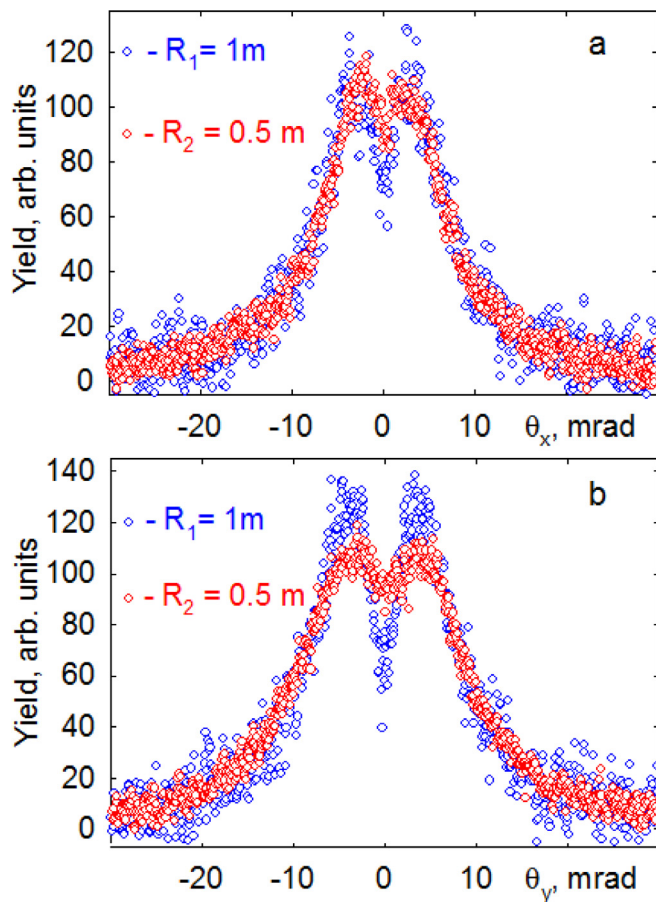
Fig. 4. (a) Horizontal and (b) vertical cross-sections of PXR angular distributions for $R_1 = 1$ m and $R_2 = 0.5$ m.

Fig. 5. (a) Horizontal and (b) vertical cross-sections of PXR angular distributions for $R_2 = 0.5$ m. △: experimental value, solid line: fitted result, and ◯: difference between them.

photon emission angle relative to the Bragg direction and varies from 10.59 keV to 12.82 keV in the observed angular range for photons of the first-order reflection, which changes the transmission fraction ratio from 0.997 to 0.993. To mitigate this effect, a thorough vacuum path from the crystal to the X-ray detector would be preferable.

The appropriate distance of the X-ray detector from the crystal is mainly determined based on the resolution of the beam size measurement and the amount of shielding of the detector from background radiation. In [19], we investigated the relation between the experimental resolution during beam size determination and the distance R_2 of the X-ray detector from the crystal, and found that the experimental resolution is almost constant for $R_2 \leq 1$ m; therefore, the detector could be placed closer to the crystal. In such case, however, the background radiation must be carefully taken into account (see [17,19] for details).

5. Conclusions

The performed measurements confirmed the effectiveness of the method for determining the electron beam size by measuring PXR angular distributions from a 255-MeV electron beam in a thin crystal for two distances between the crystal and the coordinate detector, as proposed in [18,19]. The present method is model-independent, i.e., it does not require information on the spectral-angular distribution of the detected radiation, the X-ray energy dependence of the detector efficiency, the divergence of the electron beam including the initial angular spread and the multiple scattering angle inside the crystal, or

the crystal quality. For electron energies above 5 GeV, covering the beam energies for XFEL linear accelerators, the peak intensity of the DTR angular distribution exceeds that of PXR [20]. Thus, the present diagnostic method would be applicable to electron beams of XFEL accelerators using DTR.

CRediT authorship contribution statement

A.V. Berdnichenko: Software, Validation. **Yu.A. Goponov:** Software, Validation. **R.A. Shatokhin:** Software, Validation. **Y. Takabayashi:** Conceptualization, Investigation, Writing – review & editing. **I.E. Vnukov:** Conceptualization, Software, Writing – original draft, Supervision.

Declaration of competing interest

The authors declare that they have no known competing financial interests or personal relationships that could have appeared to influence the work reported in this paper.

Acknowledgments

References

[1] R.B. Fiorito, Proceedings of PAC09, 2009, p. 741.

[2] The European X-Ray Free-Electron Laser Technical Design Report, DESY 2006-097, 2007.

[3] H. Loos, et al., Proceedings of FEL08, 2008, p. 485.

[4] ILC Technical Design Report, 2013.

[5] A Multi-TeV Linear Collider Based on CLIC Technology: CLIC Conceptual Design Report, 2012.

[6] A. Gogolev, A. Potylitsyn, G. Kube, J. Phys. Conf. Ser. 357 (2012) 012018.

[7] Y. Takabayashi, Phys. Lett. A 376 (2012) 2408.

[8] M.L. Ter-Mikaelian, High Energy Electromagnetic Processes in Condensed Media, Wiley-Interscience, New York, 1972.

[9] A.N. Didenko, B.N. Kalinin, S. Pak, A.P. Potylitsin, S.A. Vorobiev, V.G. Baryshevsky, V.A. Danilov, I.D. Feranchuk, Phys. Lett. A 110 (1985) 177.

[10] A.V. Shchagin, V.I. Pristupa, N.A. Khizhnyak, Phys. Lett. A 148 (1990) 485.

[11] S. Asano, I. Endo, M. Harada, S. Ishii, T. Kobayashi, T. Nagata, M. Muto, K. Yoshida, H. Nitta, Phys. Rev. Lett. 70 (1993) 3247.

[12] R.B. Fiorito, D.W. Rule, X.K. Maruyama, K.L. DiNova, S.J. Evertson, M.J. Osborne, D. Snyder, H. Rietdyk, M.A. Piestrup, A.H. Ho, Phys. Rev. Lett. 71 (1993) 704.

[13] P. Rullhusen, X. Artru, P. Dhez, Novel Radiation Sources using Relativistic Electrons, World Scientific, Singapore, 1998.

[14] B. Sones, Y. Danon, R.C. Block, Nucl. Instrum. Methods Phys. Res. A 560 (2006) 589.

[15] Y. Hayakawa, K. Hayakawa, K. Nogami, T. Sakai, I. Sato, Y. Sumitomo, Y. Takahashi, T. Tanaka, Phys. Rev. Accel. Beams 22 (2019) 024701.

[16] Y. Takabayashi, K. Sumitani, Phys. Lett. A 377 (2013) 2577.

[17] G. Kube, C. Behrens, A.S. Gogolev, Yu.P. Popov, A.P. Potylitsyn, W. Lauth, S. Weisse, Proceedings of IPAC2013, 2013, p. 491.

[18] I.E. Vnukov, Y.A. Goponov, M.A. Sidnin, R.A. Shatokhin, K. Sumitani, Y. Takabayashi, J. Surf. Invest.: X-Ray, Synchrotron Neutron Tech. 13 (2019) 515.

[19] Yu.A. Goponov, S.A. Laktionova, R.A. Shatokhin, M.A. Sidnin, K. Sumitani, Y. Takabayashi, I.E. Vnukov, Phys. Rev. Accel. Beams 22 (2019) 082803.

[20] Yu.A. Goponov, S.A. Laktionova, O.O. Pligina, M.A. Sidnin, I.E. Vnukov, Nucl. Instrum. Methods Phys. Res. B 355 (2015) 150.

[21] Yu.A. Goponov, R.A. Shatokhin, M.A. Sidnin, K. Sumitani, Y. Takabayashi, I.E. Vnukov, I.S. Volkov, J. Instrum. 15 (2020) C04025.

[22] Yu.A. Goponov, R.A. Shatokhin, K. Sumitani, Y. Takabayashi, I.E. Vnukov, Nucl. Instrum. Methods Phys. Res. A 996 (2021) 165132.

[23] A.S.S. Silva, C.S. Gomes, A.S. Machado, J.R. Nascimento, R.S. Santos, D.F. Oliveira, M.J. Dos Anjos, R.T. Lopes, X-Ray Spectrom. 48 (2019) 375.

[24] Y. Takabayashi, A.V. Shchagin, Nucl. Instrum. Methods Phys. Res. B 278 (2012) 78.

[25] A.L. Meadowcroft, C.D. Bentley, E.N. Stott, Rev. Sci. Instrum. 79 (2008) 113102.

[26] A.V. Berdnichenko, R.A. Shatokhin, Y. Takabayashi, I.E. Vnukov, Phys. Lett. A 409 (2021) 127537.

[27] M.J. Berger, J.H. Hubbell, S.M. Seltzer, J. Chang, J.S. Coursey, R. Sukumar, D.S. Zucker, K. Olsen, XCOM: Photon cross section database (version 1.5), 2010.